A Model for the Shear Thickening Effect of Raking Systems on Red Mud.

Charles Nadeau[1], Damien Boudeville[2], André Leclerc[3], Romain Chesnaux[4], Guy Simard[5] and Alain Boivin[6]

1. Graduate Student,
2. Graduate Student,
3. Professor,
4. Professor,
5. Professor,

Université du Québec à Chicoutimi, Chicoutimi, Québec, Canada

6. Senior Research Scientist,

Arvida Research and Development Centre, Rio Tinto, Jonquière, Québec, Canada

Corresponding author: aleclerc@uqac.ca

Abstract

Raking systems are commonly installed in settlers used in the mining industry. They contribute to the thickening of the mud and to its displacement towards the underflow. These effects have been known for many years, but the understanding of the compaction mechanisms is incomplete. A better understanding of these mechanisms would facilitate rake design improvements and would allow for a more accurate assessment of their efficiency. Several software suppliers propose commercial codes that simulate fluid flow, but unfortunately, no software application has been identified to simulate the compaction of mud by the shearing action of a rotating rake. Red mud compaction by shear action has been measured in our laboratory using a novel and unique experimental set-up. The observed data agree well with a semi-empirical mathematical model that we have established based on shear strain. This model has been incorporated as a compaction module into the ANSYS FLUENT fluid flow software to simulate the mud compaction by a rotating rake. The compacting performance of rake systems under various operational conditions can therefore be investigated.

Keywords: Red mud; shear strain thickening; compaction; rake.

1. Introduction

In the Bayer process, settlers are used for clarification and thickening of the bauxite residue. Thickener rakes contribute to the thickening of the slurry and to its displacement towards the underflow. Although the thickening action of a rake is a key issue, the understanding of the rake compaction mechanisms is still incomplete today. Buscall and White [1] have indicated that the permeability and the compressive yield stress of a concentrated suspension are factors contributing to its thickening. Usher and Scales [2] used fundamental theoretical models to predict the compressive dewaterability of thickener suspensions, based on the suspension compressive yield stress and hindered settling function. Discrepancies between predicted thickener performance and actual performance were attributed to shear processes such as raking. Farrow *et al*. [3] investigated the relative importance of compression and shear for dewatering of kaolin suspensions. They concluded that rake action, not compression, was the dominant dewatering mechanism. Du *et al*. [4] studied the effect of raking on the structure of a flocculated kaolinite suspension, and stated that:

"While forming this self-supporting structure resisting the self-weight compression, this network structure is also fragile to additional applied shear stress, evidence showed by the results from Malvern Mastersizer".

Simulation is another efficient tool available to study the efficiency of gravity thickeners. In this way Bürger *et al*. [5] and Martin [6] have studies the settling behavior of flocculated suspensions in clarifier-thickeners. Rake action was neglected in their analysis. Sutalo *et al*. [7] and Rudman *et al*. [8] have carried out Computational Fluid Dynamic (CFD) analysis of the rake transport in thickeners. Thickening by the shearing action of the rake was not included in their analysis. Shear thickening is usually excluded from most analyses because, to our knowledge, no simple relation between solid fraction and shear is available.

In this paper a novel experimental set-up that allows the solid fraction of sheared red mud to be measured as a function of an applied shear strain and a simple semi-empirical relation between solid fraction and shear strain are presented. Finally this mathematical relation has been incorporated as a compaction module into the ANSYS FLUENT fluid flow software to validate our measuring procedure of the mud shear strain and to simulate the mud compaction by a rake blade.

2. Experimental

2.1. Experimental set-up

The design of the experimental set-up used to study shear thickening requires that two major difficulties be solved: eliminate tractive rods emerging form the mud bed and establish a procedure to measure mud displacement. Tractive rods must be eliminated because they may act as dewatering pickets complicating the analysis of the data.

The experimental set-up consists of two nonmagnetic concentric cylinders, delimiting between them a circular channel. The cylinders rest on a nonmagnetic table. The outer cylinder is made of Plexiglas, so that the mud movement may be observed. A ruler tape is fixed as a length reference on the outer cylinder. A second set of such cylinders, may be added above the first set, increasing the mud capacity to study the effect of the height of the mud bed. Up to four metallic spheres or half spheres, may be symmetrically inserted on the channel bottom. They are used as magnetic rotors to shear the mud. Four electromagnets are symmetrically located on a rotating circular arc under the table. They provide the magnetic traction moving the rotors around the channel without traction rods. The speed of the rotating arc may be varied and is chosen to be representative of the typical translational speed of rakes in industrial settlers. Figure 1 shows this experimental set-up. A digital camera is placed directly in front of the apparatus to record the transits of the rotors.

Bauxite residue obtained from the Rio Tinto Vaudreuil alumina refinery was used to prepare a suspension by diluting to 75 g/L with a 20 g/L caustic solution and then flocculated in a 10 L cylinder with 60 g/t of ALT780VHM flocculant. After resting for a few hours, the supernatant liquid is removed and the remaining suspension is gently poured into the circular channel.

All the tests are carried at room temperature and a typical test lasted two hours. The effect of the speed of the rotors, of their number (1,2 or 4) and of their shape (half or complete sphere) and the effect of the mud bed height have been investigated. At intervals of ten minutes during the test, the rotors were stopped; two samples were collected in front and behind a rotor to measure their solid mass fraction by conventional means. The average of the two values was considered to be the solid mass fraction of the mud bed at the rotor position. A rheometer could be used *in situ* to measure directly the yield stress and the viscosity of the mud in the channel. After these manipulations the rotors were set into motion again.

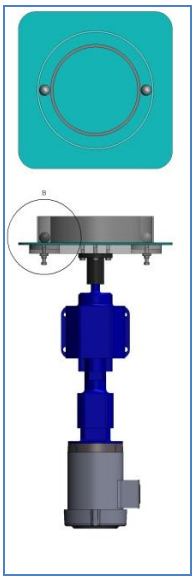

Figure 1. Experimental set-up.

2.2. Mud strain measurement

The movement of a rotor produces a wave-like deformation in the mud bed that travels along the channel. The movement of this wave is filmed by the digital camera and the recorded movie is loaded into a computer. An image recognition software is used to follow the bi-dimensional movement of an element of mud during the transit of a rotor. Only two dimensions are available because the depth dimension is not recognized by the camera. The image analysis reveals that the trajectories of the mud elements form a loop similar to the cursive letter ℓ (Figure 2). This is not surprising since the trajectories of water droplets under wave action are circles. To measure the components of the strain tensor, two neighboring mud elements are followed, with which the partial derivatives $\partial u/\partial x$, $\partial u/\partial y$, $\partial v/\partial x$ and $\partial v/\partial y$ are calculated, where u and v are the displacements of the mud elements along the x and y axes and where ∂x and ∂y are their spacing along the same axes. The spacing between the neighboring mud elements is chosen to maximize the partial derivatives. When the spacing is too great, the denominator of the derivatives grows while the numerator tends to remain constant resulting in smaller strain values, and *vice versa*. Thus there exists an optimal spacing that maximizes the strain value. The accuracy of the calculated derivatives may be increased by averaging five neighboring mud elements instead of using only one. Averaging with more than five neighbors is not warranted when comparing the extra calculation time with the extra gain in accuracy. Figure 3 shows the typical layout of the mud elements. The derivatives are calculated for the central mud element located at point O using the five neighboring mud elements located at points A, B, C, D and E. The averaging procedure is described in details by Lewis *et al*. [9]. This procedure is applied for every point (the green diamonds in Figure 2) of the trajectory of the central mud element O. Finally the magnitude of the mud strain γ for every point of the trajectory of the central element is taken as the norm of the bi-dimensional strain tensor:

$$\gamma = \sqrt{\left(\frac{\partial u}{\partial x}\right)^2 + \left(\frac{\partial u}{\partial y}\right)^2 + \left(\frac{\partial v}{\partial x}\right)^2 + \left(\frac{\partial v}{\partial y}\right)^2} \qquad (1)$$

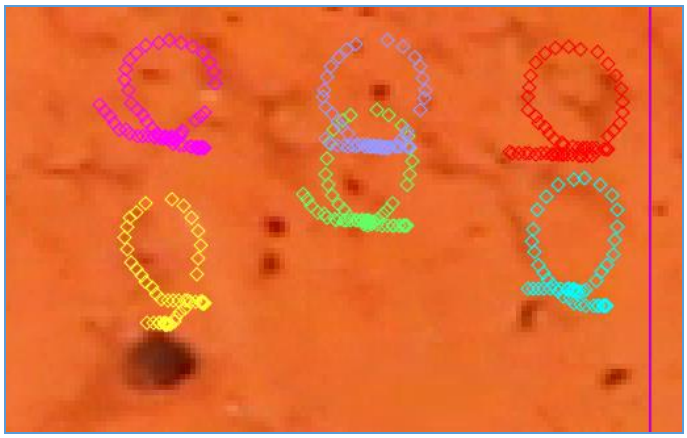

Figure 2. Typical trajectories of five mud elements.

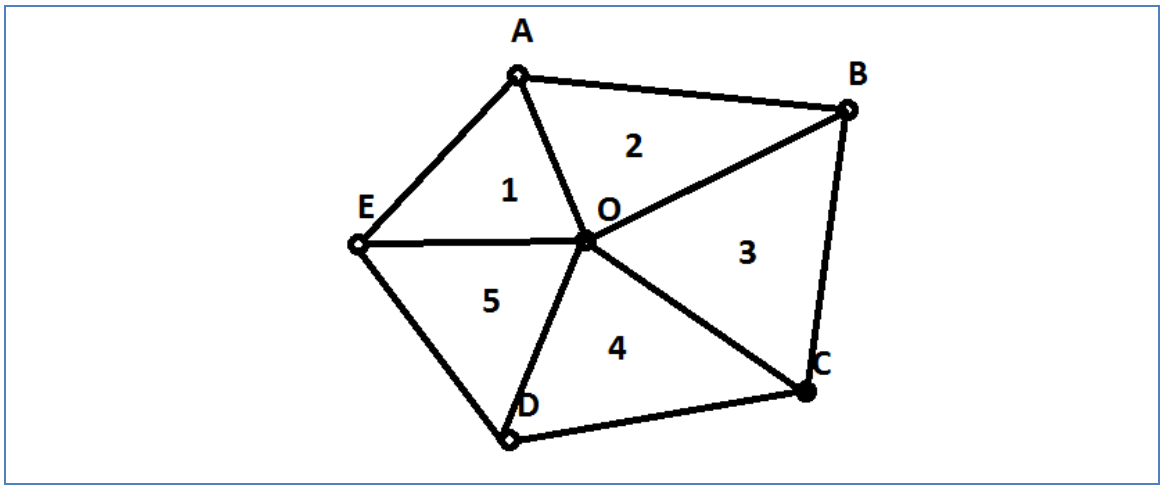

Figure 3. Layout of the points for calculating the derivatives at the central point O.

3. Results and Discussion

3.1. The shear thickening model

Figure 4 presents the data collected with one half sphere rotating at 0.5, 1 and 2 RPM in the lower channel. Similar curves were obtained for all the other cases. The error bars correspond to the 95 % confidence interval (± 0.7 %). It is obvious that the relationship is non-linear. The initial solid mass fraction is somewhat less than 42 %. It corresponds to the solid mass fraction where the compressive yield stress of the mud increases very rapidly. It depends on the flocculation process and varies slightly with the different batches of red mud suspension. The solid mass fraction increases rapidly at the beginning and then levels off around 51 %. It follows that as the mud thickens dewatering becomes more difficult.

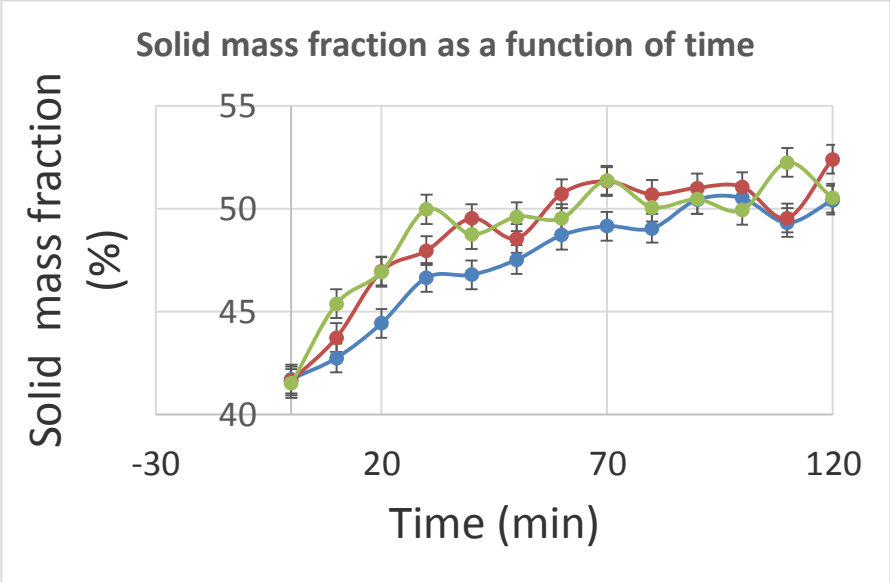

Figure 4. Shear thickening curves with one half sphere. Legend: blue 0.5 RPM; red 1 RPM; green 2 RPM.

These observations suggest the following model for shear thickening. The rate of change of the density should be inversely proportional to the density. From the mechanics of deformable continua, shear rate is related to the fluidity of a continuum through its viscosity and shear strain is related to the rigidity (or the elasticity) of the continuum through its shear modulus. As suggested by Du *et al*. [4] the shear thickening is related to modifications to the mud structure. Because rigidity and elasticity are structural properties, we propose that shear strain instead of shear rate should be used to evaluate shear thickening. The rate of change of the density should then be proportional to the shear strain. Hence the rate of change of the density may be written as:

$$\frac{dX}{dt} = \frac{k_1 \gamma}{X} \tag{2}$$

where: X Solid mass fraction, %
γ Strain, unit less
k_1 Empirical constant, %^{2}/sec

The empirical constant k_1 is related to the rheological properties of the mud. Rearranging Equation (2) as differentials and integrating:

$$X dX = k_1 \gamma dt \tag{3}$$

$$X^2 = X_0^2 + 2k_1 \int_0^t \gamma dt = X_0^2 + 2k_1 \gamma_M t \tag{4}$$

where: X0 Initial solid mass fraction, %
γ_M Mean strain, unitless
t Duration of strain, sec

Equation (4) is valid as long as the duration time is not too long because the mass fraction cannot exceed unity, whereas in Equation (4) the mass fraction grows indefinitely with time! To overcome this difficulty the second right hand term is replaced by

$$\frac{2k_1'\int_0^t \gamma dt'}{k_2 + \int_0^t \gamma dt'} \tag{5}$$

where: k_1' Empirical constant, $\%^2$
k_2 Empirical constant, sec.

The empirical constants k_1' and k_2 are related to the rheological properties of the mud. The limit of this term is:

$$\lim_{t' \to \infty} \frac{2k_1'\int_0^{t'} \gamma dt'}{k_2 + \int_0^{t'} \gamma dt'} = 2k_1' \tag{6}$$

With this modified second right hand term Equation (4) becomes:

$$X^2 = X_0^2 + \frac{2k_1'\int_0^{t'} \gamma dt'}{k_2 + \int_0^{t'} \gamma dt'} = X_0^2 + \frac{2k_1'\gamma_m t}{k_2 + \gamma_m t} \tag{7}$$

The maximum density achievable by shear thickening is obtained by taking the limit of Equation (7):

$$X_{\max} = \sqrt{X_0^2 + 2k_1'} \tag{8}$$

Let us define the unit less variable z:

$$z = \frac{\int_0^t \gamma dt'}{k_2 + \int_0^t \gamma dt'} \tag{9}$$

Equation (7) then becomes:

$$X^2 = X_0^2 + 2k_1'z \tag{10}$$

The data from Figure 4 are plotted in Figure 5 using X^2 as ordinate and z as abscissa. The 95 % confidence interval that corresponds to ± 0.7 % is approximately ± 70 $\%^2$. Linear regressions fit the data well with correlation coefficients of 0.955, 0.924 and 0.888 for the 0.5, 1 and 2 RPM curves respectively. A value of 12 sec was used for the constant k_2. The correlation coefficients of the fits are not very sensitive to the value of k_2. From Equation 8 the maximum densities achievable are 53.0, 53.8 and 53.8 % for the 0.5, 1 and 2 RPM cases respectively. When a single straight line, not shown in the figure, is fitted through all the data, a correlation coefficient of 0.893 and a maximum density of 53.6 % are obtained. Figure 6 is a plot of all the data collected from all the tests: one, two or four half spheres or full spheres at all RPM values. A value of 12 sec for the constant k_2 maximized the correlation coefficient of the linear regression with a correlation coefficient of 0.809, a k_1' value of 518.55 $\%^2$ and a maximum density of 52.3 %. A large proportion of the vertical scatter originates from the scatter in the initial densities.

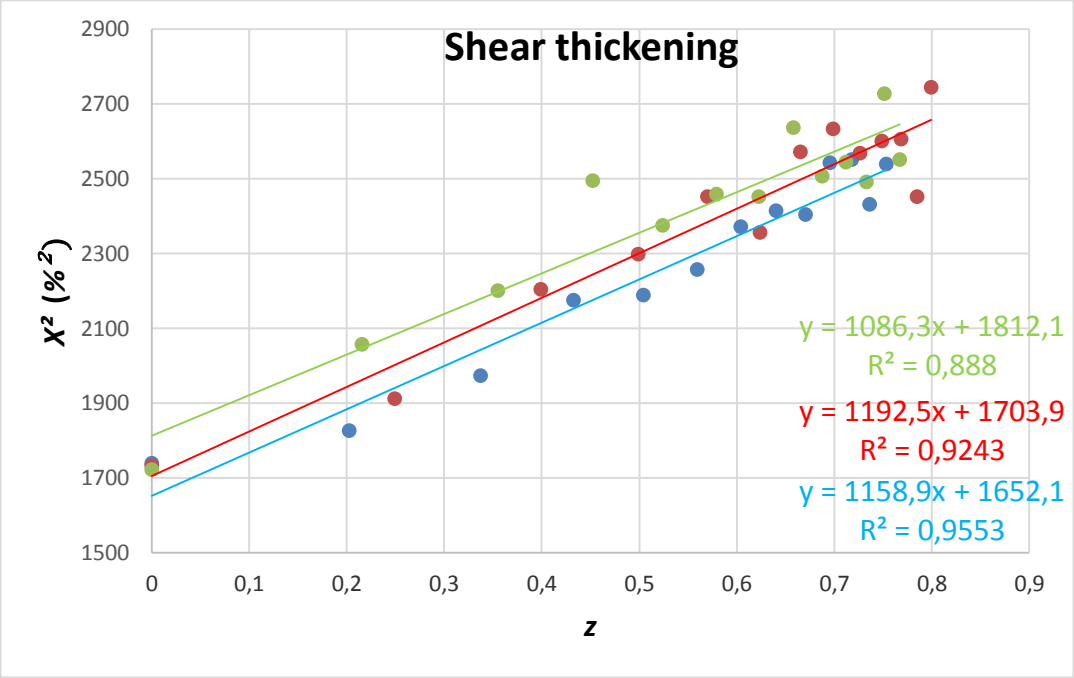

Figure 5. Shear thickening curves with one half sphere. Legend: blue 0.5 RPM; red 1 RPM; green 2RPM.

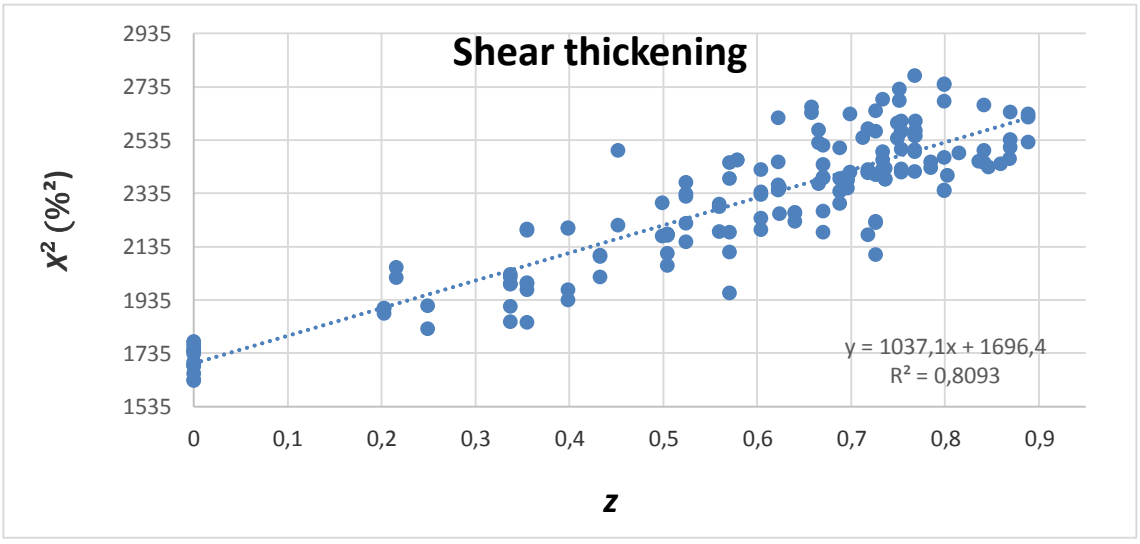

Figure 6. Shear thickening curve. The data include all the tests.

3.2. Effect of the mud bed height

The effect of the bed height was investigated by tripling the cylinder height. The solid mass fractions were measured at the base of the channel and at two thirds of the mud bed height. Figure 7 presents the data collected with four half spheres rotating at 1 RPM. The blue line corresponds to the data collected at the base of the mud bed and the red line corresponds to the data collected in the upper third of the mud bed. At the base of this high mud bed, thickening is faster than in the case of the original mud bed experiments with one half sphere at 1 RPM (see red line in Figure 4). This is expected since four half spheres generate more strain than one half sphere. The maximum density achieved at the base of the deep mud bed is 52.7 % compared

with 52.4 % for the shallow mud bed. Thus the effect of the bed height is insignificant to the end compaction within the accuracy of the data. This is not surprising in view of the large values of the compressive yield stress for solid mass fractions greater than 40 %. In the upper third of the mud bed, thickening is quite slow because the shear strain is weak in that region.

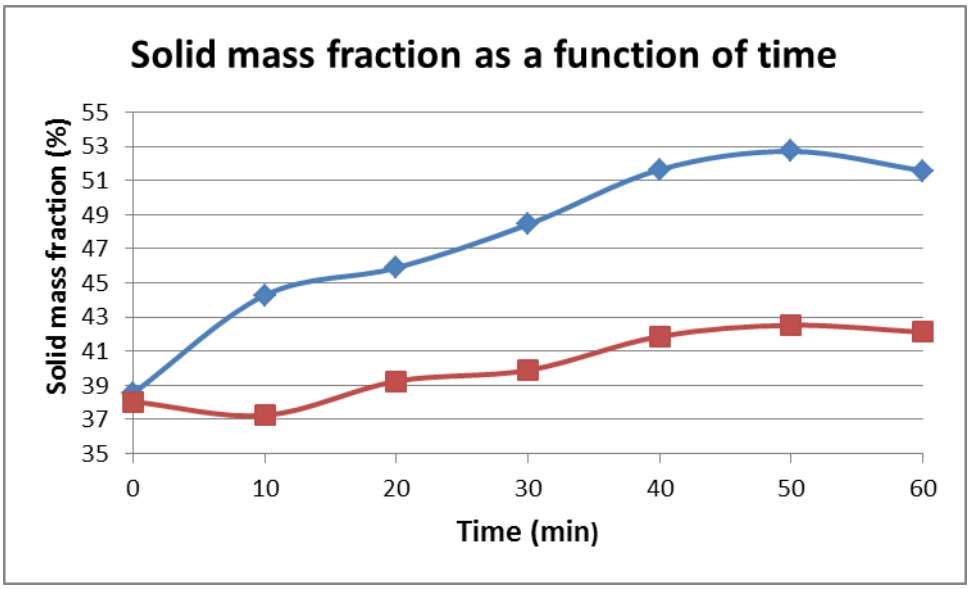

Figure 7. Thickening curves in the deep mud bed. The blue data originate from the base of the mud bed and the red data originate from the upper third of the mud bed.

3.3. ANSYS FLUENT fluid flow simulation

The rotation of the half ball at 0.5, 1 and 2 RPM in the experimental set-up was simulated using the ANSYS FLUENT fluid flow software. The simulation was carried in two dimensions only because the experimental shear strains are bi-dimensional. Shear rates at the mesh points is one of the output of this simulation. The shear strains were obtained by multiplying the shear rate by the time step of the simulation. These shear strains were used in Equation 10 to calculate the mud density at each time steps. Figure 8 shows the correlation between the simulated and the measured values. The agreement is remarkable, validating the experimental procedure that was used to measure the mud strain. Moreover the thickening by a bi-dimensional rake blade, 4 cm long and 1 mm thick, inclined at 45^{o} and rotating at 2 RPM, was simulated. Figure 9 compares the thickening effect of this blade with that of the half sphere. The thickening by the blade is slightly faster. Thus the strain induced by the blade is larger than that induced by the half sphere. The maximum densities are the same, which is expected from Equation 10. When the strain is larger, the maximum density is only achieved more rapidly. Its value depends on the rheological properties of the mud, not on the shape of the rotor.

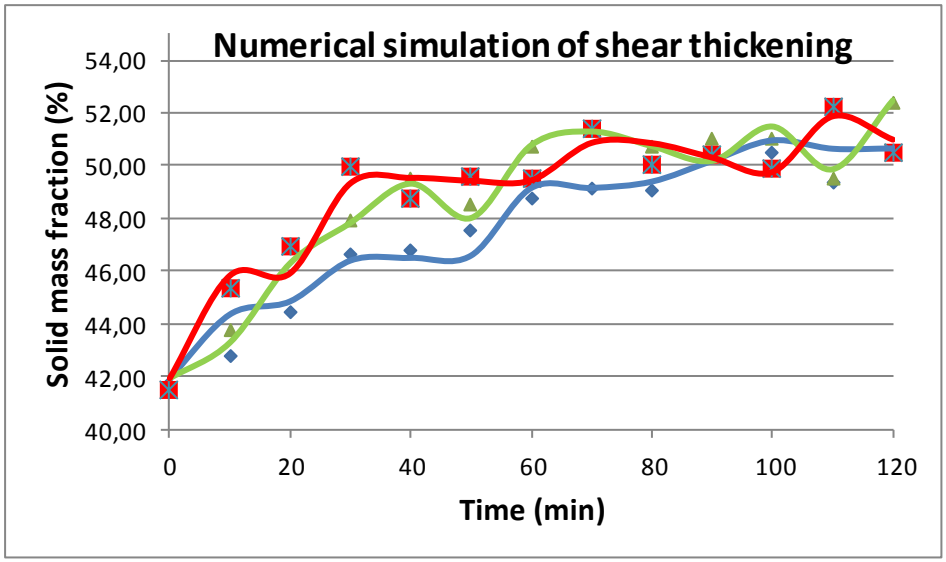

Figure 8. Comparison of the numerical simulation (full curves) with the measured values (points). Legend: blue 0.5 RPM; green 1 RPM; red 2 RPM.

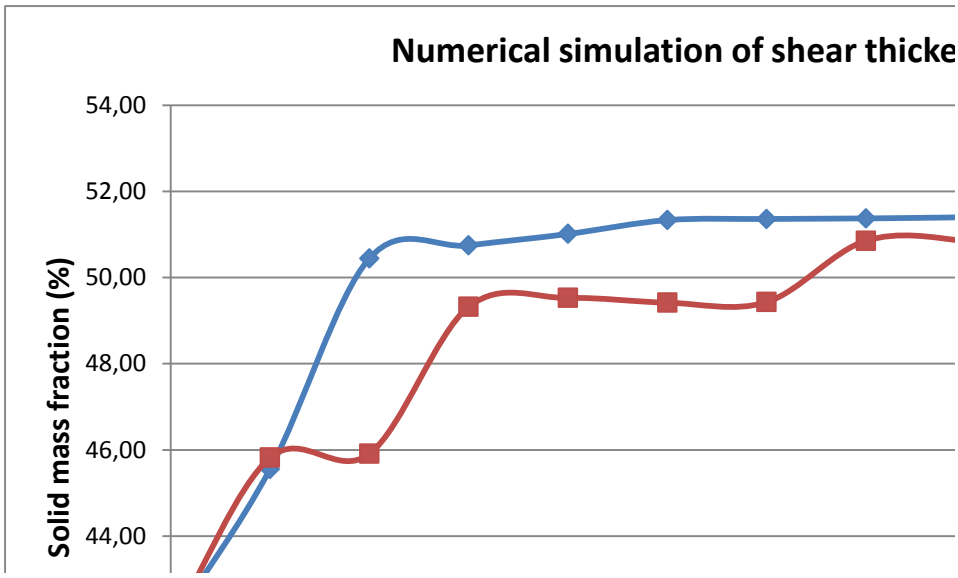

Figure 9. Numerical simulation of shear thickening by the blade of a rake (upper curve) and by the half ball (lower curve).

4. Conclusions and Future Work

A simple semi-empirical mathematical relationship implying directly only shear strain, not shear rate, and its duration time fits well the shear thickening data collected with our novel experimental apparatus. Two empirical constants that depend on the rheological properties of the red mud also appear in this relationship. From this, it appears that the shape of the shearer is not important, as long as the amount of shear that it produces is measurable or calculable. The maximum shear thickening achievable does not depend on the shape of the shearer but on the rheological properties of the slurry, although the time taken to reach this maximum value will be shorter for efficient shearers. This mathematical relationship may be incorporated in simulation software to calculate shear thickening in thickeners.

The effect of dewatering rods could be examined by fixing such a vertical rod on the top of the rotors used in our experimental set-up. Moreover, extra work is required to relate the empirical constants from the mathematical relationship to the rheological properties of the red mud.

5. Acknowledgements

This work was performed with the financial and in-kind support of Rio Tinto, who kindly permitted the publication of this paper. Thanks are also due to the Government of Canada and the Government of Québec for the two granted MITACS scholarships.

6. References

1. R. Buscal and L.R. White, The consolidation of concentrated suspensions, *Journal of the Chemical Society Faraday Transactions*. I. 83, (1987), 873-891.
2. Shane P. Usher and Peter J. Scales, Steady state thickener modelling from the compressive yield stress and hindered settling function, *Chemical Engineering Journal*. Vol. 111, (2005), 253-261.
3. J.B. Farrow et al., Consolidation and aggregation during gravity thickening, *Chemical Engineering Journal*. Vol. 80, (2000), 141-148.
4. Jianhua Du et al., A cryo-SEM study of aggregate structure changes during clay setting and raking processes, *International Journal of Mineral Processing*. Vol. 93, (2009), 66-72.
5. Raimund Burger et al., Mathematical model and numerical simulation of the dynamics of flocculted suspensions in clarifier-thickeners, *Chemical Engineering Journal.* Vol. 111, (2005), 119-134.
6. A.D. Martin, Optimisation of clarifier-thickeners processing stable suspensions for turn-up/turn-down, *Water Research.* Vol. 38, (2004), 1568-1578.
7. I.D. Sutalo et al., Flow visualisation and computational prediction in thickener rake models. *Minerals Engineering.* Vol. 16, (2003), 93-102.
8. M. Rudman et al., Efficiency of raking in gravity thickeners, *International Journal of Mineral Processing.* Vol. 95, (2010), 30-39.
9. Roland W. Lewis et al., Fundamentals of the finite element method for heat and fluid flow, *John Wiley & Sons, Ltd.*(2004), 341pp.